Path Planning and Tracking for Vehicle Collision Avoidance Based on Model Predictive Control With Multiconstraints

Jie Ji, Amir Khajepour, Wael William Melek, *Senior Member, IEEE*, and Yanjun Huang

***Abstract*—A path planning and tracking framework is presented to maintain a collision-free path for autonomous vehicles. For path-planning approaches, a 3-D virtual dangerous potential field is constructed as a superposition of trigonometric functions of the road and the exponential function of obstacles, which can generate a desired trajectory for collision avoidance when a vehicle collision with obstacles is likely to happen. Next, to track the planned trajectory for collision avoidance maneuvers, the path-tracking controller formulated the tracking task as a multiconstrained model predictive control (MMPC) problem and calculated the front steering angle to prevent the vehicle from colliding with a moving obstacle vehicle. Simulink and CarSim simulations are conducted in the case where moving obstacles exist. The simulation results show that the proposed path-planning approach is effective for many driving scenarios, and the MMPC-based path-tracking controller provides dynamic tracking performance and maintains good maneuverability.**

***Index Terms*—Autonomous vehicle, collision avoidance, model predictive control (MPC), multiconstraints, path planning, path tracking.**

I. Introduction

OWING to the rapid increase in traffic density, vehicle safety has become a crucial factor in modern intelligent transportation systems. While passive safety systems, in combination with ever-increasing active safety systems in motor vehicle, have been developed to avoid vehicle crashes and minimize the impact of accidents [1], the need for further reduction in traffic accident incidences using modern control and sensing technologies remains of great interest. In recent years, autonomous vehicles have attracted strong attention from the automotive industry, due to their potential applications in collision avoidance. However, fully autonomous driving for the objective of having "zero accidents on the road" remains a complex task. Further work, such as planning the path upon detecting obstacles, and controlling the actuators so that the vehicle follows the planned path, is often required before the collision avoidance system is road-ready.

Although there has been substantial research on path planning and tracking in collision avoidance systems for unmanned aerial vehicles (UAV) and other robots [2]–[5], it is not easy to apply these approaches directly to vehicle collision scenarios, since the vehicle can only move at the limits of its stability and handling capability in a constrained environment. Furthermore, to solve the collision avoidance problems on the road, it is also necessary to consider other moving vehicles that have their own motion properties.

The path planning for a vehicle collision avoidance system is to generate a collision-free trajectory, which takes into consideration geometric characteristics of obstacles and the kinematic constraints of the autonomous vehicle [6]. Early works on path planning for autonomous vehicles date back to the 1980s and were primarily focused on computing a time-optimal and collision-free trajectory going from a given point to another [7], [8]. Since then, many different computational methods and various successful implementations have been reported in the literature.

The common path-planning methods include A* heuristic search, visibility graph method, generalized Voronoi diagram, and artificial potential field (APF) [6]. The APF method was inspired by classical mechanics; it formulates a relationship between the motion of the autonomous vehicle and the sum of the applied forces [9]. This method has been used to generate repulsive potential fields to obstacles and attractive potential fields to the goal, which enables the vehicle to avoid collisions with obstacle boundaries, while proceeding toward its goal. The APF-based method is very different from previously mentioned approaches, which have all future path information known after the planner's execution and before the vehicle's motion [10]. However, traditional APF-based path-planning approaches possess an inherent problem, which is the formation of local minimum that may prevent the vehicle from arriving at the target [11].

In this paper, a new 3-D potential field that can generate collision-free trajectory for autonomous vehicle is developed based on the boundary conditions of the road and the vehicle's kinematic model. Collision avoidance conditions are established, and the algorithm can be updated in real time to obtain

Manuscript received February 17, 2015; revised September 14, 2015 and December 23, 2015; accepted March 22, 2016. Date of publication April 22, 2016; date of current version February 10, 2017. The work of J. Ji was supported in part by the National Natural Science Foundation of China under Grant 61304189, by the Fundamental Research Funds for the Central Universities under Grant XDJK2015B028, and by the Basic and Cutting-Edge Research Projects in Chongqing under Grant cstc2015jcyjA60007. The work of A. Khajepour, W. W. Melek, and Y. Huang was supported by the Natural Sciences and Engineering Research Council of Canada. The review of this paper was coordinated by Prof. J. Wang.

J. Ji is with the College of Engineering and Technology, Southwest University, Chongqing 400715, China (e-mail: jijiess@163.com).

A. Khajepour, W. W. Melek, and Y. Huang are with the Department of Mechanical and Mechatronics Engineering, University of Waterloo, Waterloo, ON N2L 3G1, Canada (e-mail: a.khajepour@uwaterloo.ca; william.melek@uwaterloo.ca; y269huan@uwaterloo.ca).

Color versions of one or more of the figures in this paper are available online at http://ieeexplore.ieee.org.

Digital Object Identifier 10.1109/TVT.2016.2555853

a collision-free trajectory in a complex workspace involving static and dynamic obstacles.

A successful collision avoidance maneuver does not end with only path planning but extends to path tracking that aims to ensure that the vehicle will follow a planned trajectory as close as possible [12].

The commonly used methods for path tracking of autonomous vehicle include fuzzy logic [13], sliding-mode control [14], and robust control [15]. However, many of these control applications assumed that the calculated inputs would never reach the saturation limits of the actuators; however, in practice, this is not true. Moreover, vehicles are made up of mechanical and electrical parts, which are also subjected to physical constraints. Thus, nonlinear characteristics of vehicles and their interactions with the road must be considered. The model predictive control (MPC) is an attractive method to tackle this problem [16]. Because of its capability to systematically handle input constraints and admissible states, MPC with multiconstraints is adopted to track the planned trajectory for collision avoidance in this work.

Here, the path-tracking problem is formulated as an MPC problem with multiconstraints. At each sampling time instant, a future input sequence of front steering angle for collision avoidance can be calculated in a defined horizon. This is accomplished by solving a finite-time optimal control problem, considering a set of constraints in both the control actions and the plant outputs [16]. An additional feature of an MPC-based approach for collision avoidance is that it continuously optimizes the performance index by receiving information about vehicle position, heading angle, and obstacles as the vehicle moves [17].

This paper presents a path-planning approach based on the theory of virtual potential field and a path-tracking framework using multiconstrained MPC (MMPC) for autonomous vehicles, which seeks to minimize the incidence for collision on roads. By receiving information about vehicle position, road parameters, and obstacles surrounding the vehicle, this framework provides a vehicle trajectory for a collision avoidance system based on a 3-D virtual dangerous potential field, which seeks to minimize risk to the vehicle through evasive maneuvering. A MMPC-based path-tracking system, considering the geometric constraints of road and dynamic constraints of the vehicle, calculates the steering wheel angle to track the planned trajectory and to avoid obstacles. Simulations in different scenarios show the effectiveness of the proposed approach. In particular, MPC with constraint of the steering angle is compared with the proposed approach, in terms of performance and constraint satisfaction.

The remainder of this paper is organized as follows: In the next section, the problem and overall framework of the collision avoidance system are introduced. Section III describes the path-planning algorithm that determines a collision-free trajectory based on the 3-D dangerous potential field. Section IV develops the augmented vehicle dynamic model used for path tracking. Section V presents the main contribution of this work and details MMPC. The effectiveness of the proposed framework is demonstrated through simulations in Section VI. Finally, conclusions are provided in Section VII.

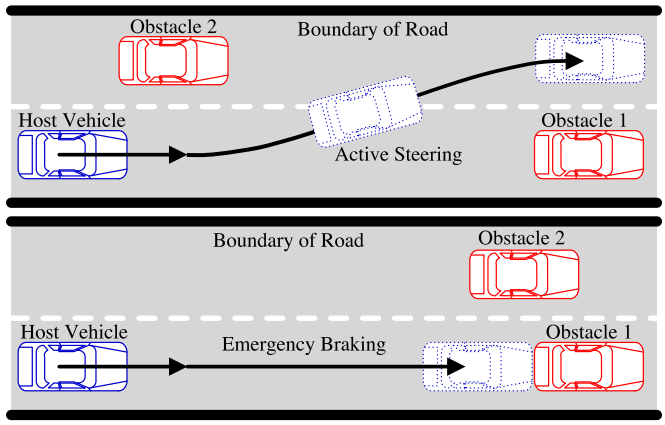

Fig. 1. Problem description of collision avoidance on road.

II. Description of Collision Avoidance System

A. Problem Description

The majority of traffic accidents on roads are caused by vehicle collision. The objective of any collision avoidance system is to design a vehicle control algorithm to avoid an imminent accident. Longitudinal control (i.e., emergency braking only) and lateral control (i.e., active steering only) are possible choices of actuation configuration for collision avoidance maneuver [18]. Fig. 1 represents the two aforementioned maneuvers.

It is becoming increasingly common for luxury cars to be fitted with an emergency brake assist or brake assist system. However, longitudinal collision avoidance controllers are of limited benefit for preventing head-on collisions between road vehicles traveling at high speed or for rear-end collisions when there is insufficient separation between the vehicles. Under these circumstances, aggressive lateral vehicle maneuvers are more appropriate, as is altering the path of the vehicle to move it out of danger. The maneuvers in this case can be completed in a shorter distance than that required to stop the vehicle. This paper focuses purely on the steering control of an autonomous vehicle to track the planned trajectory and to perform an emergency collision avoidance maneuver.

B. Framework of Collision Avoidance System

The proposed collision avoidance framework aims to generate a collision-free trajectory at any instance and keeps the vehicle as close as possible to the planned trajectory. The trajectory is updated at the same control cycle to handle any changes in the obstacles' locations and speeds. The overall proposed architecture is presented in Fig. 2.

The architecture in Fig. 2 describes the main elements of a collision avoidance system, which is composed of three blocks: the collision-free trajectory generator, the path-tracking control system, and the virtual simulation environmental model.

The path-planning block in this architecture generates a collision-free trajectory during runtime. In the case of a vehicle traveling on the road, it can be planned based on occurrence of certain events, e.g., a stationary obstacle or moving vehicle is detected in the path. Moreover, the referenced signals of lateral position, yaw rate, and sideslip angle of the simplified model

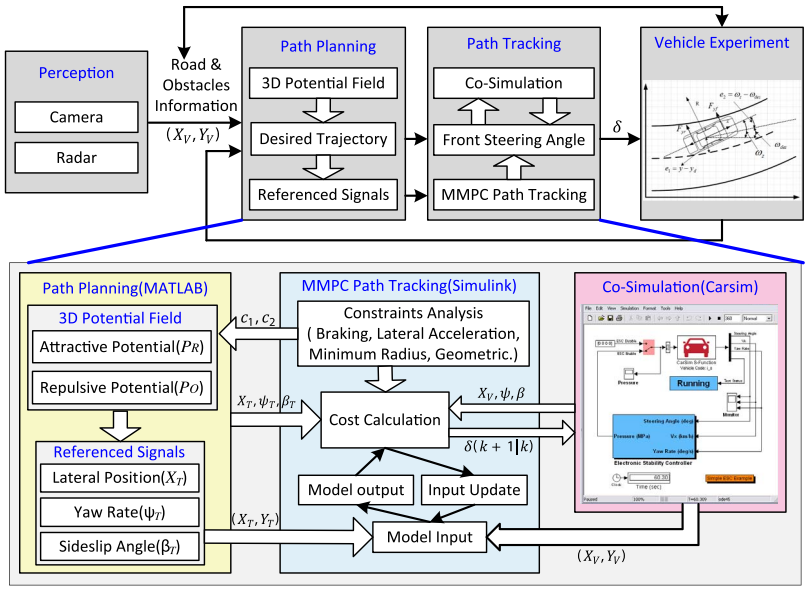

Fig. 2. Overall architecture of collision avoidance system.

are the state variables for MMPC that can be calculated from the planned trajectory in this block.

The path-tracking module is based on a receding horizon control design [19]. The tracking problem is formulated as a constrained optimization problem. The cost function penalizes lateral tracking errors between the predicted position of vehicle and the planned trajectory derived of the 3-D potential field. Furthermore, the penalty of the yaw rate tracking errors will play a main role in the cost function when the yaw rate error exceeds its threshold. Regarding the vehicle sideslip regulation, the desired sideslip is simply defined via a tolerance band around the sideslip angle (β_{curv}) that also takes into account the sign of the rate of sideslip angle (β_{curv}).

In simulations presented in this paper, the control inputs obtained by the path-tracking block are applied to the CarSim vehicle model. CarSim is software, which builds full nonlinear models of actual vehicles when parameters, such as dimensions of the vehicle platform, specifications of the engine and tires, and coefficients of the suspensions, are known. The CarSim vehicle model has been validated with experimental results on an actual vehicle [21]. For simplicity, it is assumed that all vehicle variables, brake torques, tire forces, and the surface friction coefficient are available to the controller by direct measurements or through the estimation algorithm in CarSim.

III. Path Planning for Collision Avoidance Using 3-D Virtual Dangerous Potential Field

This section focuses on formulating a path-planning algorithm for the collision avoidance system based on 3-D virtual dangerous potential field. Many researchers have studied path planning for autonomous vehicle, and a number of rule-based methods have been proposed, such as virtual desired trajectory [20], [21] and elastic band theory [22], etc. However, driving is a complex task, and even highway subtleties make the implementation of a rule-based planning algorithm cumbersome.

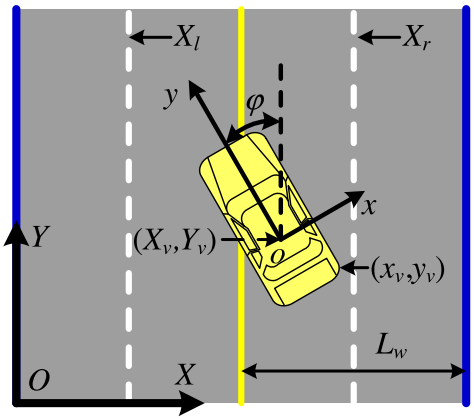

Fig. 3. Fixed earth and vehicle body axis systems.

Therefore, utilizing an APF for local trajectory planning offers an elegant alternative [23]. This method can modify the collision-free trajectory in real time. Hence, potential function approaches have already seen considerable use for path planning of autonomous vehicle [24].

To simplify the derivation of the collision-free trajectory using the potential field approach, this paper assumes the following conditions [25], as illustrated in Fig. 1.

- The road is straight with road boundaries on both sides.
- Only a single obstacle appears in front of the host vehicle when it is in motion.
- Regardless of vehicle avoidance action, the obstacle continues moving along the road.

Two coordinate systems, i.e., vehicle body and fixed earth, respectively, are shown in Fig. 3. The vehicle body coordinate system is a right-hand orthogonal axis set (x, o, y) centered on the vehicle's center of mass, with y defined positive forward along the centerline of the vehicle and x defined positive to the right [26]. Since this axis system moves with the vehicle, it is not useful for measuring vehicle position relative to the ground.

Therefore, a fixed earth coordinate system (X, O, Y) is defined to be colocated and aligned with the vehicle axis at some point before the start of any maneuver but does not subsequently move or rotate with the vehicle. The coordinates of vehicle's center of mass in the fixed earth coordinate system are (X_v, Y_v). The X-axis is along the perpendicular of lane centerline, whereas Y-axis is in the direction of lane centerline. With the aforementioned assumptions, both the road and the vehicle's motion state are described in the fixed earth coordinate system. The horizontal angle of rotation between these axis systems is the vehicle heading angle φ, X_l and X_r are the coordinates of centerline of left and right lanes in the X-direction of the fixed earth coordinate system, and L_w denotes the width of each lane.

The proposed universal potential $P_U(X, Y)$ is obtained by adding the repulsive potential $P_O(X, Y)$ resulting from all obstacles and the attractive potential $P_R(X, Y)$ resulting from the target trajectory, where each fulfills a particular role in the path-planning task [27].

To present the mathematical function of the potential field, the potential of the road in the absence of obstacles will be presented first. The attractive potential of the road $P_R(X, Y)$ prevents the vehicle from drifting off the highway and guides the vehicle into the center of its lane, but it is also small enough to be easily overcome in the case that a lane change is necessary for collision avoidance. The mathematical expression of the potential function expressed in the fixed earth coordinate system is considered as

$$P_R(X, Y) = A(X)A(Y) + P_A(X, Y). \tag{1}$$

The function has two maximums related to the road boundaries and two minimums related to the centerlines of both lanes. $A(X)$ and $A(Y)$ determine the amplitudes of the potential field along the width and length of road, respectively. $P_A(X, Y)$ denotes an attractive potential driving the autonomous vehicle forward in the region of universal potential field and leading the vehicle toward the centerline of the right lane when it has passed the obstacles ahead. A form for the functions $A(X)$, $A(Y)$, and $P_A(X, Y)$ can be considered as (2)–(4), shown at the bottom of the page, where P_m indicates the amplitude of potential of the middle line of the road; Y_o is the position of obstacle in the Y-direction of the fixed earth axis system; D_b is the shortest braking distance of the "big sedan" model in CarSim, and it can be calculated by (8); D_t and D_s denote the scope of the repulsive and universal potential fields for collision avoidance in the Y-direction of the fixed earth axis system, respectively.

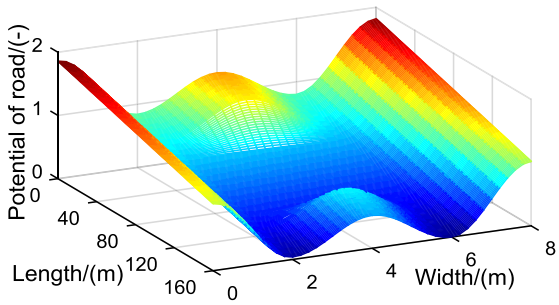

Fig. 4. Three-dimensional attractive potential field of the road.

The 3-D graphical representation of the function defined in (1) is illustrated in Fig. 4.

For the potential of an obstacle or leading vehicle, a cost function using the information of the distance and angle to the detected obstacles from the vehicle is used for generating the repulsive potential field. The potential must be shaped to keep the vehicle at a safe distance from any obstacle and also encourage lane changing if there is not enough longitudinal space for the host vehicle to avoid the obstacle by braking. The mathematical expression of a potential function for an obstacle or a leading vehicle can be expressed in the fixed earth axis system as

$$P_O(X, Y) = \frac{\left| e^{-c_1(X-X_o)^2 - c_2(Y-Y_o)^2} - P_t \right|}{1 - P_t} \tag{5}$$

where X_o is the position of obstacle in the X-direction of the fixed earth axis system; parameters c_1, c_2, and P_t determine the value and the shape of the potential field associated with the relative speed and distance between the vehicle and the obstacle. P_t denotes the threshold that determines the scope of the repulsive potential field, c_1 is the weight on the lateral distance between the vehicle and the obstacle, and c_2 corresponds to the distance between the obstacle and the point from where the collision avoidance maneuver started. c_1 and c_2 can be described as

$$c_1 = \begin{cases} \dfrac{-\ln(P_t) - c_2(Y-Y_0)^2}{\left\{0.5 * L_w * \left[\sin\left(\frac{Y-Y_0+D_b}{D_b} * \pi - \frac{\pi}{2}\right) + 1\right]\right\}^2}, & |Y - Y_o| \le D_b \\ 0, & \text{else} \end{cases} \tag{6}$$

$$c_2 = -\frac{\ln(P_t)}{D_b^2} = -\frac{64F_m^2 \ln(P_t)}{\left[m(V^2 - v^2) + 4F_m L_l\right]^2} \tag{7}$$

$$D_b = \frac{m(V^2 - v^2)}{8F_m} + \frac{L_l}{2} \tag{8}$$

$$A(X) = \frac{\left[|\mathrm{sgn}(X - X_l) + \mathrm{sgn}(X - X_r)|\,(1 - P_m) + 2P_m\right]\left[\cos\left(\frac{2\pi X}{L_w}\right) + 1\right]}{4} \tag{2}$$

$$A(Y) = \begin{cases} 0, & |Y - Y_o| \le D_b \\ \frac{|Y-Y_o| - D_b}{D_t - D_b}, & D_b < |Y - Y_o| \le D_t \\ 1, & \text{else} \end{cases} \tag{3}$$

$$P_A(X, Y) = \frac{|X - X_r| + |Y - (Y_o + 0.5D_s)|}{100} \tag{4}$$

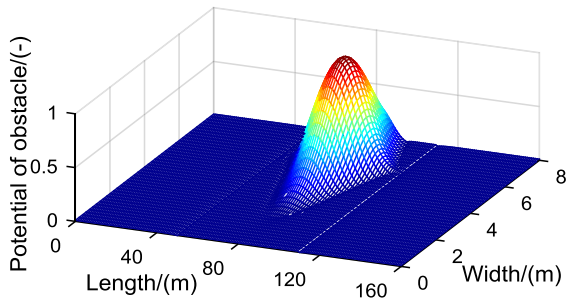

Fig. 5. Three-dimensional repulsive potential field of obstacle.

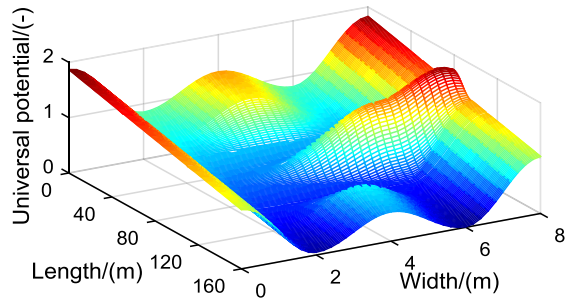

Fig. 6. Universal potential field of road and obstacle.

where m is the mass of the vehicle; V and v are the longitudinal velocity at the center of gravity (CG) of vehicle and obstacle, respectively; F_m denotes the maximum braking force of each tire; and L_l is the outside diameter of the obstacle.

The 3-D graphical representation of the function (5) is illustrated in Fig. 5.

If the attractive potential $P_R(X,Y)$ and repulsive potential $P_O(X,Y)$ are added together, the universal potential function $P_U(X,Y)$ will be

$$P_U(X,Y) = P_R(X,Y) + P_O(X,Y). \tag{9}$$

Fig. 6, which shows the 3-D map of the universal potential field, displays the threats around the autonomous vehicle on the road at a particular instant in time.

The negative gradient of universal potential field is defined as induced force, which is the steepest descent direction for guiding the vehicle to the target point. Energy of the collision threats is minimized by following the direction of the induced force.

Because the autonomous vehicle is attracted by the road potential and repelled by the obstacle potential, the universal induced force $\overrightarrow{F_U}$ is the sum of an attractive force $\overrightarrow{F_R}$ and a repulsive force $\overrightarrow{F_O}$, whose direction indicates the most promising local direction of motion. The desired motion of the autonomous vehicle from any given position can be determined by the induced force $\overrightarrow{F_U}$, as defined in Fig. 7.

As shown in Fig. 7, the universal induced force of vehicle is given by

$$\begin{aligned}\overrightarrow{F_U} &= -\nabla P_U(X_v,Y_v) = -\nabla P_R(X_v,Y_v) - \nabla P_O(X_v,Y_v)\\ &= (\overrightarrow{F_{RX}} + \overrightarrow{F_{RY}}) + (\overrightarrow{F_{OX}} + \overrightarrow{F_{OY}})\end{aligned} \tag{10}$$

where $\overrightarrow{F_{RX}}$ and $\overrightarrow{F_{OX}}$ are the attractive force and repulsive force in the X-direction. $\overrightarrow{F_{RY}}$ and $\overrightarrow{F_{OY}}$ are the attractive force and repulsive force in the Y-direction. They can be expressed as

$$\begin{aligned}&[\overrightarrow{F_{RX}} \quad \overrightarrow{F_{RY}} \quad \overrightarrow{F_{OX}} \quad \overrightarrow{F_{OY}}]\\ &= \left[\frac{-\partial[P_R(X_v,Y_v)]}{\partial X} \quad \frac{-\partial[P_R(X_v,Y_v)]}{\partial Y}\right.\\ &\quad \left.\times \frac{-\partial[P_O(X_v,Y_v)]}{\partial X} \quad \frac{-\partial[P_O(X_v,Y_v)]}{\partial Y}\right].\end{aligned} \tag{11}$$

$X_T(k)$, $\beta_T(k)$, and $\psi_T(k)$ are the reference information of planned trajectory, sideslip angle, and yaw angle at instance time k, which can be derived by taking small steps in the direction of the universal induced force $\overrightarrow{F_U}$. The 2-D contour plot of the resulting universal potential displays the desired collision-free trajectory for path tracking of the vehicle, as shown in Fig. 8.

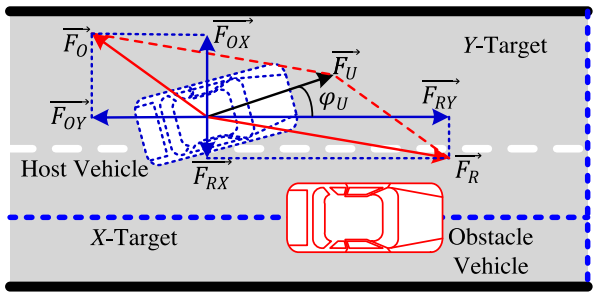

Fig. 7. Direction of reduced force.

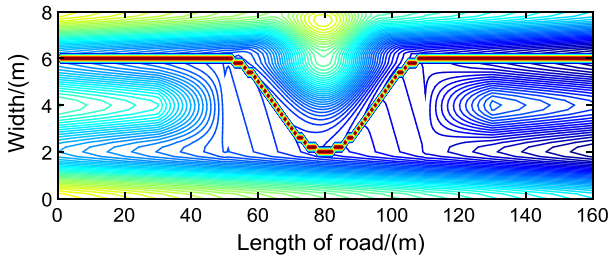

Fig. 8. Contour plot of the potential field and collision-free trajectory.

IV. Vehicle Mathematical Model for Path-Tracking Problem

The path-tracking problem is very dependent on the vehicle modeling since it is a requirement for MMPC law design. The model used in this paper should take into account the kinematic and dynamic aspects of the vehicle [16]. Here, we present an augmented mathematical model of a vehicle used for the development of a collision avoidance system. Section IV-A develops a vehicle dynamic model along with its lateral and yaw dynamics, and Section IV-B introduces a discrete state-space vehicle model used for the development of an MMPC.

A. Vehicle Dynamic Model for Path Tracking

This section describes the vehicle and tire models that we used for control design. For the path-tracking problem, the following assumptions are made in the vehicle model: 1) The longitudinal velocity of vehicle is constant; 2) at the front and

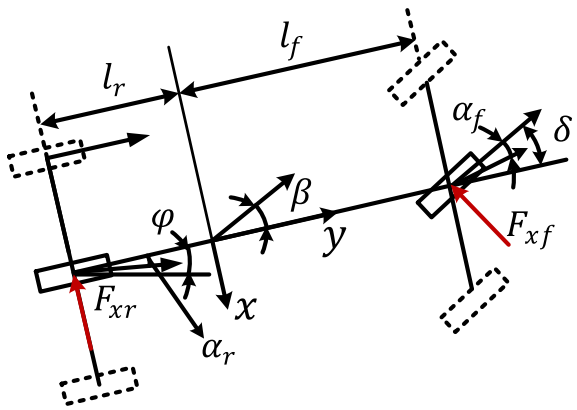

Fig. 9. Vehicle dynamics model used for path tracking.

rear axles, the left and right wheels are lumped in a single wheel; and 3) suspension movements, slip phenomena, and aerodynamic influences are neglected.

With these assumptions, the linear dynamic model of a conventional vehicle, as shown in Fig. 9, is obtained according to Newton's laws. Using the body sideslip angle β and the yaw rate of vehicle body $\dot{\psi}$ as state variables, the vehicle lateral dynamics can then be described by

$$mV(\dot{\beta}+\dot{\psi}) = F_{xf} + F_{xr} \tag{12}$$

$$I_z\ddot{\psi} = {}_fF_{xf} - l_rF_{xr} \tag{13}$$

where I_z is the vehicle moment of inertia about the yaw axis; l_f and l_r are the longitudinal distances from the CG of vehicle to the front and rear wheels, respectively.

There exist a number of different models for cornering tire forces. For small tire slip angles, the lateral tire forces are approximated as a linear function of tire slip angle. The front and rear tire forces F_{xf}, F_{xr} and tire slip angles α_f, α_r are defined as [28]

$$F_{xf} = C_f \times \alpha_f = C_f \times \left(\delta - \beta - \frac{l_f\dot{\psi}}{V}\right) \tag{14}$$

$$F_{xr} = C_r \times \alpha_r = C_r \times \left(-\beta + \frac{l_r\dot{\psi}}{V}\right) \tag{15}$$

where δ is the front-wheel steering angle; C_f and C_r represent the linearized cornering stiffness of the front and rear wheels, respectively.

Substituting (14) and (15) into (12) and (13), the equations governing the lateral and yaw dynamics in a vehicle model can be expressed as

$$\dot{\beta} = \frac{-(C_r+C_f)}{mV}\beta + \left(\frac{C_rl_r - C_fl_f}{mV^2} - 1\right)\dot{\psi} + \frac{C_f}{mV}\delta \tag{16}$$

$$\ddot{\psi} = \frac{C_rl_r - C_fl_f}{I_z}\beta - \frac{C_rl_r^2 + C_fl_f^2}{I_zV}\dot{\psi} + \frac{C_fl_f}{I_z}\delta. \tag{17}$$

B. Discrete Linear Vehicle Model for MPC

Here, we derive a discrete state-space vehicle model, for the MMPC optimization process, from the mathematical model obtained in the previous section. In the new vehicle model, the state-space vector is made up of the lateral position of the vehicle CG X_v, the vehicle sideslip angle β, the yaw angle ψ, and the yaw rate $\dot{\psi}$. The input is given by the angle of front wheel δ. With this definition, the state-space vector is obtained as follows:

$$X_c = [X_v \quad \beta \quad \psi \quad \dot{\psi}]^T. \tag{18}$$

The state equations can be written based on (16) and (17) derived in the previous section as

$$\dot{X}_c = A_cX_c + B_c\delta \tag{19}$$

$$Y_c = C_cX_c \tag{20}$$

where

$$A_c = \begin{bmatrix} 0 & V & V & 0 \\ 0 & -\frac{C_r+C_f}{mV} & 0 & \frac{C_rl_r-C_fl_f}{mV^2} - 1 \\ 0 & 0 & 0 & 1 \\ 0 & \frac{C_rl_r-C_fl_f}{I_z} & 0 & -\frac{C_rl_r^2+C_fl_f^2}{I_zV} \end{bmatrix}$$

$$B_c = \begin{bmatrix} 0 \\ \frac{C_f}{mV} \\ 0 \\ \frac{C_fl_f}{I_z} \end{bmatrix},\ C_c = \begin{bmatrix} 1 & 0 & 0 & 0 \\ 0 & 1 & 0 & 0 \\ 0 & 0 & 0 & 1 \end{bmatrix}. \tag{21}$$

The aforementioned vehicle model is a linearized, continuous-time, and single-input and multiple-output system. However, the system to be controlled is usually modeled by a discrete state-space model in the MPC literature [29]. Therefore, (19) and (20) are transformed into a discrete state-space model to obtain

$$X_d(k+1) = A_dX_d(k) + B_du(k) \tag{22}$$

where A_d and B_d are the state and control matrices for the discrete state-space equation, respectively, which can be calculated with the Euler method as

$$A_d = e^{A_C\Delta T} \tag{23}$$

$$B_d = \int_{k\Delta T}^{(k+1)\Delta T} e^{A_C[(k+1)\Delta T-\tau]}B_C d\tau \tag{24}$$

where ΔT is the sampling interval for the discrete state-space model.

The lateral displacement, sideslip angle, and yaw rate of vehicle are defined as outputs using

$$Y_d(k) = C_dX_d(k) \tag{25}$$

where

$$Y_d(k) = \begin{bmatrix} X_v \\ \beta \\ \dot{\psi} \end{bmatrix}, C_d = C_c = \begin{bmatrix} 1 & 0 & 0 & 0 \\ 0 & 1 & 0 & 0 \\ 0 & 0 & 0 & 1 \end{bmatrix}. \tag{26}$$

In path tracking using MMPC, it is common to formulate the constrained control problem as a real-time optimization problem subject to hard constraints on plant variables and soft constraints on outputs. The discrete state-space model (22) and (25) are augmented as uniform model with integrators [29].

Let us denote the difference of the state variables and the control variable by

$$\Delta X_d(k+1) = X_d(k+1) - X_d(k) \tag{27}$$
$$\Delta X_d(k) = X_d(k) - X_d(k-1) \tag{28}$$
$$\Delta u(k) = u(k) - u(k-1). \tag{29}$$

Substituting (27)–(29) into (22) and (25) transforms the latter two equations into a discrete state-space model with the increments of the variables $X_d(k)$ and $u(k)$ as

$$\Delta X_d(k+1) = A_d \Delta X_d(k) + B_d \Delta u(k) \tag{30}$$
$$Y_d(k+1) - Y_d(k) = C_d A_d \Delta X_d(k) + C_d B_d \Delta u(k). \tag{31}$$

Note that the input to the state-space model and the output equations is $\Delta u(k)$. To connect $\Delta X_d(k)$ to the outputs $Y(k)$, a new state variable vector is chosen as

$$X_a(k) = \begin{bmatrix} \Delta X_d(k) \\ Y_d(k) \end{bmatrix}. \tag{32}$$

Combining (32) with (30) and (31) yields the following state-space model:

$$X_a(k+1) = A_a X_a(k) + B_a \Delta u(k) \tag{33}$$
$$Y_a(k) = C_a X_a(k) \tag{34}$$

where the triplet (A_a, B_a, C_a) are called the augmented model, which can be described as follows:

$$A_a = \begin{bmatrix} A_d & O_a^T \\ C_d A_d & I_a \end{bmatrix},\ B_a = \begin{bmatrix} B_d \\ C_d B_d \end{bmatrix},\ C_a = \begin{bmatrix} O_a I_a & \end{bmatrix}$$
$$O_a = \begin{bmatrix} 0 & 0 & 0 & 0 \\ 0 & 0 & 0 & 0 \\ 0 & 0 & 0 & 0 \end{bmatrix},\ I_a = \begin{bmatrix} 1 & 0 & 0 \\ 0 & 1 & 0 \\ 0 & 0 & 1 \end{bmatrix}. \tag{35}$$

V. Design of Multiconstrained Model Predictive Control

The path-tracking task can be posed as a predictive control problem with the constraints derived from vehicle dynamics and kinematics. The analysis presented here is based on [29] but adapted to suit the vehicle collision avoidance application.

A. Prediction of State and Output Variables

An important step in the design of an MPC for path tracking is to predict the future behavior of the vehicle at each time step. This future prediction determines the control inputs within a specified prediction horizon, and on the basis of these future states, a performance index is minimized to compute the optimal control inputs [12].

Here, we assume that the current time is k, $k > 0$; the prediction horizon is $N_p = 10$ as the length of the optimization window and the control horizon is $N_c = 5$. The state variable vector $X_a(k)$ provides the current plant information, which is available through measurement.

With given information $X_a(k)$, the future state variables can be predicted for N_p steps ahead, as follows:

$$X_a(k+1), \ldots, X_a(k+m), \ldots, X_a(k+N_P) \tag{36}$$

where $X_a(k+m)$ is the predicted state variable at $k+m$ with given current plant information $X_a(k)$.

We denote by ΔU_m the sequence of future input increments computed at time k for the current observed states. That is

$$\Delta U_m = [\Delta u(k), \ldots, \Delta u(k+m), \ldots, \Delta u(k+N_c-1)]^T. \tag{37}$$

Using the set of future control parameters ΔU_m and the state-space model (A_a, B_a, C_a), the state variables of the vehicle are calculated sequentially by continuing the iteration of (33) as follows:

$$\begin{aligned} X_a(k+1) &= A_a X_a(k) + B_a \Delta u(k) \\ X_a(k+2) &= A_a^2 X_a(k) + A_a B_a \Delta u(k) + B_a \Delta u(k+1) \\ &\vdots \\ X_a(k+N_c) &= A_a^{N_C} X_a(k) + A_a^{N_C-1} B_a \Delta u(k) + \cdots \\ &\quad + B_a \Delta u(k+N_C-1) \\ &\vdots \\ X_a(k+N_P) &= A_a^{N_P} X_a(k) + A_a^{N_P-1} B_a \Delta u(k) + \cdots \\ &\quad + A_a^{N_P-N_C} B_a \Delta u(k+N_C-1). \end{aligned} \tag{38}$$

By using successive substitution, it is assumed that the control input varies for only the N_c time steps (the control horizon) and then is held constant up to the preview horizon [30], [31].

We then define the state vector and predicted outputs for the predictive state-space model as

$$\begin{aligned} X_m(k) &= X_a(k) \\ &= \left[\Delta X_v(k)\ \Delta\beta(k)\ \Delta\psi(k)\ \Delta\dot{\psi}(k)\ X_v(k)\ \beta(k)\ \dot{\psi}(k)\right]^T \end{aligned} \tag{39}$$
$$Y_m(k) = [Y_a(k+1) \quad \cdots \quad Y_a(k+N_p)]^T. \tag{40}$$

In this situation, it is straightforward to derive the prediction model of performance outputs over the prediction horizon N_P in a compact matrix form as

$$Y_m(k) = F_m X_m(k) + G_m \Delta U_m \tag{41}$$

where

$$F_m = \begin{bmatrix} C_a A_a & C_a A_a^2 & \cdots & C_a A_a^{N_C} & \cdots & C_a A_a^{N_P} \end{bmatrix}^T_{3N_P \times 7} \tag{42}$$

$$G_m = \begin{bmatrix} C_a B_a & 0 & \cdots & 0 \\ C_a A_a B_a & C_a B_a & \cdots & 0 \\ \vdots & \vdots & \cdots & 0 \\ C_a A_a^{N_C-1} B_a & C_a A_a^{N_C-2} B_a & \cdots & C_a B_a \\ \vdots & \vdots & \ddots & \vdots \\ C_a A_a^{N_P-1} B_a & C_a A_a^{N_P-2} B_a & \cdots & C_a A_a^{N_P-N_C} B_a \end{bmatrix}_{3N_P \times N_C}.$$

B. Development of Cost Function With Vehicle Dynamics

As described in Section III, the reference location information of planned trajectory $P_r(k)$, sideslip angle $\beta_r(k)$, and yaw

rate $\dot{\psi}_r(k)$ at time k are chosen as the given set-point information for MMPC, which are calculated by the universal potential field of road and obstacles within the prediction horizon N_P. The reference signals are described as follows:

$$\begin{bmatrix} P_r(k) & \beta_r(k) & \psi_r(k) \end{bmatrix} = \begin{bmatrix} X_T(k+1) & \beta_T(k+1) & \psi_T(k+1) \\ X_T(k+2) & \beta_T(k+2) & \psi_T(k+2) \\ \cdots & \cdots & \cdots \\ X_T(k+N_p) & \beta_T(k+N_p) & \psi_T(k+N_p) \end{bmatrix}. \quad (43)$$

The objective of MMPC is to bring the predicted outputs $P_v(k)$, $\beta_v(k)$, and $\dot{\psi}_v(k)$ as close as possible to the set-point signals. We define the cost function J_E that reflects the control objective as

$$\begin{aligned} J_E =& [P_r(k) - P_v(k)]^T [P_r(k) - P_v(k)] + [\beta_r(k) - \beta_v(k)]^T \\ & \times [\beta_r(k) - \beta_v(k)] + \left[\dot{\psi}_r(k) - \dot{\psi}_v(k)\right]^T \left[\dot{\psi}_r(k) - \dot{\psi}_v(k)\right] \\ & + \Delta U_m^T \overline{R} \Delta U_m \end{aligned} \quad (44)$$

where, as in MMPC notation, $P_v(k)$, $\beta_v(k)$, and $\dot{\psi}_v(k)$ are the predicted sequence of lateral position, sideslip angle, and yaw rate of vehicle in the fixed earth coordinate system, which can be calculated for N_P time steps at time k using (34), and ΔU_m is the predicted optimization vector. $\bar{R} = r_w I_{N_C \times N_C} (r_w > 0)$ denotes the cost function matrix associated with the future values of the steer input.

Consider the autonomous vehicle traveling with constant longitudinal velocity V on the planned trajectory, and assume that the curvature of the planned trajectory is C_T at instant time k [28]. The reference sideslip angle of the vehicle is automatically determined by

$$\beta_{\text{curv}} = C_T \left(L_r - \frac{L_f m V^2}{2 C_r L} \right) \quad (45)$$

$$C_T = \frac{\left| \frac{d^2 X_T}{d Y_T^2} \right|}{\left[1 + \left(\frac{d X_T}{d Y_T} \right)^2 \right]^{\frac{3}{2}}} \quad (46)$$

where $L = L_f + L_r$ is used to denote the wheelbase of the vehicle; X_T, Y_T are the coordinates of the planned trajectory in the fixed earth coordinate system, which are derived from the universal potential field.

Following [32] and [33], we require β_{curv} to be limited in the interval $[-\beta_{\max}, \beta_{\max}]$, where

$$\beta_{\max} = \begin{cases} 2\frac{k_1 - k_2}{V_r^3} V^3 - 3\frac{k_1 - k_2}{V_r^2} V^2 + k_1, & \text{if } V < V_r \\ k_2, & \text{if } V \geq V_r \end{cases} \quad (47)$$

and V_r is the characteristic speed. Reasonable values for parameters k_1 and k_2 are $\pi/18$ and $\pi/60$, respectively [32].

When $|\beta(k)| > |\beta_{\max}|$, a regulation level $\beta_{\text{ref}} = \beta_{\max}$ ($\beta_{\text{ref}} = -\beta_{\max}$) is activated. Thus, we define the reference signal of sideslip angle as

$$\beta_r(k) = \begin{cases} \beta_{\max}, & \beta_r(k) > \beta_{\max} \\ \beta_{\text{curv}}, & \beta_r(k) \in [-\beta_{\max}, \beta_{\max}] \\ -\beta_{\max}, & \beta_r(k) < -\beta_{\max}. \end{cases} \quad (48)$$

Define the yaw rate $\dot{\psi}_{\text{curv}}$ of the desired orientation of autonomous vehicle as

$$\dot{\psi}_{\text{curv}} \approx V \cdot C_T / \cos \beta_{\text{curv}}. \quad (49)$$

For the lateral stability of the vehicle, a constraint of the maximum yaw rate ($\dot{\psi}_{\max}$) is defined, using the friction coefficient μ, gravity g, and the longitudinal velocity V, as

$$\dot{\psi}_{\max} = \frac{\mu g}{V}. \quad (50)$$

We define the reference signal of yaw rate as

$$\dot{\psi}_r(k) = \begin{cases} \dot{\psi}_{\max}, & \dot{\psi}_r(k) > \dot{\psi}_{\max} \\ \dot{\psi}_{\text{curv}}, & \dot{\psi}_r(k) \in [-\dot{\psi}_{\max}, \dot{\psi}_{\max}] \\ -\dot{\psi}_{\max}, & \dot{\psi}_r(k) < -\dot{\psi}_{\max}. \end{cases} \quad (51)$$

In the aforementioned cases, only for $|\beta(k)| > |\beta_{\max}|$ and $|\dot{\psi}(k)| > |\dot{\psi}_{\max}|$, the penalties of yaw rate and sideslip angle tracking errors will increase sharply and play a main role in the cost function.

Suppose that the reference signals $R_r(k)$ from the universal potential field and the predicted outputs in $Y_m(k)$ for path tracking are described as

$$R_r(k) = \begin{bmatrix} X_T(k+1) \\ \beta_T(k+1) \\ \dot{\psi}_T(k+1) \\ \vdots \\ X_T(k+N_p) \\ \beta_T(k+N_p) \\ \dot{\psi}_T(k+N_p) \end{bmatrix}, \; Y_m(k) = \begin{bmatrix} X_v(k+1) \\ \beta(k+1) \\ \dot{\psi}(k+1) \\ \vdots \\ X_v(k+N_p) \\ \beta(k+N_p) \\ \dot{\psi}(k+N_p) \end{bmatrix}. \quad (52)$$

Equation (44) can then be written as

$$J_E = [R_r(k) - Y_m(k)]^T [R_r(k) - Y_m(k)] + \Delta U_m^T \overline{R} \Delta U_m. \quad (53)$$

C. Constraint Analysis for MPC

There are three major types of constraints encountered in the path tracking. The first two deal with constraints imposed on the control variables, and the third deals with output constraints.

According to the kinematics and dynamics of vehicle model, the constraints, which are imposed on steering angle and stability, for the path-tracking problem are specified as

$$-C_1 \Delta \delta^{\max} \leq \Delta U_m \leq C_1 \Delta \delta^{\max} \quad (54)$$

$$-C_1 \delta^{\max} \leq C_1 u(k-1) + C_2 \Delta U_m \leq C_1 \delta^{\max} \quad (55)$$

$$C_3 \begin{bmatrix} X^{\min} \\ -\beta^{\max} \\ -\dot{\psi}^{\max} \end{bmatrix} \leq F_m X_m(k) + G_m \Delta U_m \leq C_3 \begin{bmatrix} X_{\max} \\ \beta^{\max} \\ \dot{\psi}^{\max} \end{bmatrix} \quad (56)$$

where $\delta^{\max}$ and $\Delta \delta^{\max}$ are the constraints of inputs, and $X^{\max}$ and $X^{\min}$ are the coordinate values of left and right boundaries

of road in the X-direction. Thus

$$C_1 = \begin{bmatrix} 1 \\ 1 \\ \vdots \\ 1 \\ 1 \end{bmatrix}_{Nc\times 1}, \; C_2 = \begin{bmatrix} 1 & 0 & \cdots & 0 & 0 \\ 1 & 1 & \cdots & 0 & 0 \\ \vdots & \vdots & \ddots & \vdots & \vdots \\ 1 & 1 & \cdots & 1 & 0 \\ 1 & 1 & \cdots & 1 & 1 \end{bmatrix}_{NC\times Nc}$$

$$C_3^T = \begin{bmatrix} 1 & 0 & 0\cdots 1 & 0 & 0 \\ 0 & 1 & 0\cdots 0 & 1 & 0 \\ 0 & 0 & 1\cdots 0 & 0 & 1 \end{bmatrix}_{3N_F\times 3} \tag{57}$$

subject to the inequality constraints

$$\begin{bmatrix} M_1 \\ M_2 \\ M_3 \end{bmatrix} \Delta U_m \leq \begin{bmatrix} N_1 \\ N_2 \\ N_3 \end{bmatrix} \tag{58}$$

where the data matrices are given by

$$M_1 = \begin{bmatrix} -C_2 \\ C_2 \end{bmatrix}, M_2 = \begin{bmatrix} -I \\ I \end{bmatrix}, \; M_3 = \begin{bmatrix} -G_m \\ G_m \end{bmatrix}$$

$$N_1 = \begin{bmatrix} C_1\delta^{\max} + C_1u(k-1) \\ C_1\delta^{\max} - C_1u(k-1) \end{bmatrix}, \; N_2 = \Delta\delta^{\max}\begin{bmatrix} C_1 \\ C_1 \end{bmatrix}$$

$$N_3 = \begin{bmatrix} -C_3 \begin{bmatrix} X^{\min} \\ -\beta^{\max} \\ -\dot{\psi}^{\max} \end{bmatrix} + F_m X_m(k) \\ C_3 \begin{bmatrix} X^{\max} \\ \beta^{\max} \\ \dot{\psi}^{\max} \end{bmatrix} - F_m X_m(k) \end{bmatrix}. \tag{59}$$

D. Numerous Solution Using Hildreth's Quadratic Programming Procedure

The next stage is to calculate the future steering inputs that optimize the path-tracking response of the vehicle. We present the following objective function J_E and the constraints, by combining (41), (53), and (58), as follows:

$$J_E = \frac{1}{2}\Delta U_m^T E_m \Delta U_m + \Delta U_m^T F_m \tag{60}$$

$$M_m \Delta U_m \leq N_m \tag{61}$$

where $M_m = [M_1 \; M_2 \; M_3]^T$, $N_m = [N_1 \; N_2 \; N_3]^T$, and E_m, F_m are compatible matrices and vectors in the quadratic programming problem, as follows:

$$E_m = 2\left(G_m^T G_m + \overline{R}\right) \tag{62}$$

$$F_m = -2{G_m}^T\left[R_r(k) - F_m X_m(k)\right]. \tag{63}$$

To minimize the objective function subject to inequality constraints, let us consider the following Lagrange expression [29]:

$$J_L = \frac{1}{2}\Delta U_m^T E_m \Delta U_m + \Delta U_m^T F_m + \lambda^T(M_m \Delta U_m - N_m). \tag{64}$$

The dual problem to the original primal problem is derived as

$$\max_{\lambda\geq 0} \min_{\Delta U_m} (J_L). \tag{65}$$

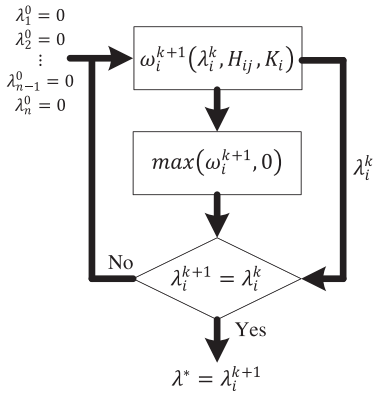

Fig. 10. Hildreth's quadratic programming for MMPC.

From the first derivative of the cost function J_L, the minimization over ΔU_m is unconstrained and is attained by

$$\Delta U_m = -E_m^{-1}\left(F_m + M_m^T\lambda\right). \tag{66}$$

Substituting this in (65), the dual problem becomes a quadratic programming problem with λ as the decision variable. The dual problem is written as

$$\min_{\lambda\geq 0}\left(\frac{1}{2}\lambda^T H_m \lambda + \lambda^T K_m + \frac{1}{2}\lambda^T E_m^{-1}\lambda\right) \tag{67}$$

where matrices H_m and K_m are given by

$$H_m = M_m E_m^{-1} M_m^T \tag{68}$$

$$K_m = N_m + M_m E_m^{-1} F_m. \tag{69}$$

Hildreth's quadratic programming procedure was adopted for solving the optimal Lagrange multipliers that minimize the dual objective function [34]. At a given step in the process, we adjust a single component λ_i in vector λ^* to minimize the objective function. The calculation process of λ^* is shown in Fig. 10; see [29] and [35] for details on convergence and implementation. Replacing the decision variable λ in (66) with the Lagrange multipliers λ^*, we have

$$\Delta U_m = -E_m^{-1}\left(F_m + M_m^T\lambda^*\right). \tag{70}$$

VI. Simulations of Path Tracking in Different Scenarios Using CarSim and Simulink

To investigate the performance of the proposed framework presented in Section II, numerical simulations with the MMPC have been conducted using vehicle simulation software, i.e., CarSim, and MATLAB/Simulink. Fig. 11 shows the block diagram of the implementation. In this architecture, a high-fidelity "big sedan" model in CarSim is used. The MMPC built in the MATLAB/Simulink is used to run a closed-loop steering maneuver to track the planned trajectory introduced in Section III. It should be pointed out that the same controller can be used to control the vehicle during different maneuvers.

This set of simulations represents a collision avoidance emergency maneuver, in which the vehicle is following the planned trajectory with a given initial forward speed. The control input

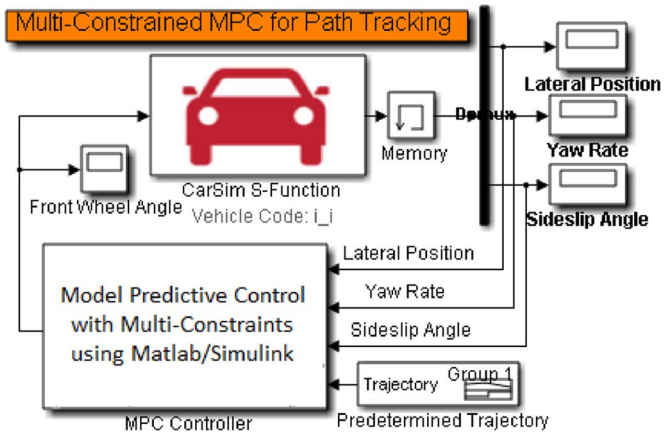

Fig. 11. Architecture of MMPC for path tracking.

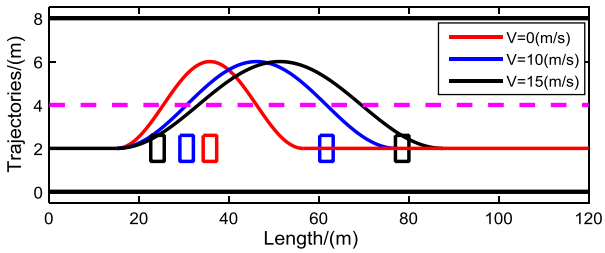

Fig. 12. Planned trajectories for path tracking.

is the steering angle of front wheels, and the goal is to follow the trajectory as close as possible by minimizing the vehicle deviation from the target path. In this context, we assume that future vehicles would be able to identify obstacles on the road, such as an animal, rock, or fallen tree/branch, and follow the desired trajectory automatically with a fully autonomous steering system.

Section VI-A describes details of the simulation scenario, and Section VI-B presents our most important results and findings from simulations.

A. Scenario Description

In the following section, we will refer to a general MPC system with constraint on the front steering angle as controller A, and the proposed MPC system, with input constraint on the steering angle of front wheel and state constraints on lateral tracking error, yaw rate, and sideslip angle, as controller B. The simulation results of controller A are reported and compared with the simulation results of controller B. The sample time in the simulations of path planning and path tracking are 0.2 and 0.1 s, respectively.

In the first scenario, suppose that a leading vehicle is moving on a straight lane with constant velocity (15, 10, and 0 m/s), i.e., less than the velocity of the host vehicle (20 m/s); this will lead to a collision with the leading vehicle. According to the current position and velocity of the leading vehicle, an alternative trajectory can be generated by the path-planning program on the basis of 3-D virtual dangerous potential field, as shown in Fig. 12.

In the second scenario, the initial velocity of the host vehicle is taken as 20 m/s, and the leading vehicle is placed at 17.5 m ahead of the host vehicle. Fig. 13(a) shows the predefined acceleration of the leading vehicle, and Fig. 13(b) shows the predefined speed command for the leading vehicle and speed response to the command in the software of CarSim. Applying the aforementioned information into the proposed 3-D dangerous potential field, a planned trajectory for collision avoidance will be generated, as shown in Fig. 13(c).

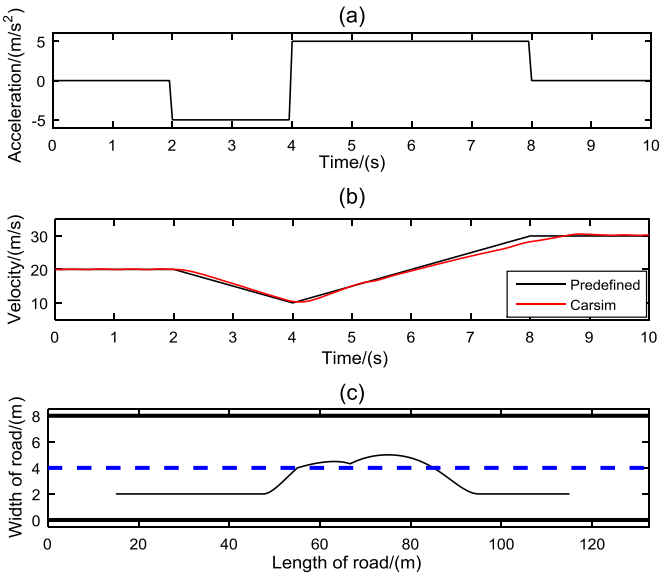

Fig. 13. Predefined information for path tracking. (a) Acceleration of leading vehicle. (b) Velocities of leading vehicle. (c) Planned trajectory derived from the 3-D potential field for scenario 2.

TABLE I
VEHICLE MODEL PARAMETERS

Symbol	DESCRIPTION	Value[units]
m	Total vehicle mass	2020[kg]
I_z	Yaw moment of inertia	3234[kg · m^2]
V	Velocity of vehicle	20[m/s]
l_f	C.g. distance to front wheels	1.40[m]
l_r	C.g. distance to rear wheels	1.65[m]
C_f	Front wheel cornering stiffness	1420[N/deg]
C_r	Rear wheel cornering stiffness	1420[N/deg]

B. Simulation Results

Table I defines the vehicle model parameters.

Scenario 1: When the leading vehicle is moving at the speed of 10 m/s, the host vehicle at a constant velocity of 20 m/s is controlled to track the planned red trajectory in Fig. 12 and is continuously checked to see whether the vehicle will collide with the obstacle.

Figs. 14–16 show the performance comparison, trajectory response, and vehicle response for the designed MPC-based path-tracking controller A and controller B, respectively. Before passing the obstacle ($0\,\text{s} \le t \le 2.5\,\text{s}$), we observe that both controllers track the paths to avoid the obstacle by turning left. After passing the obstacle ($2.5\,\text{s} \le t \le 6\,\text{s}$), both controllers bring the vehicle to the centerline of the right lane. In Fig. 14, controller B exhibits a better path-tracking ability than that of

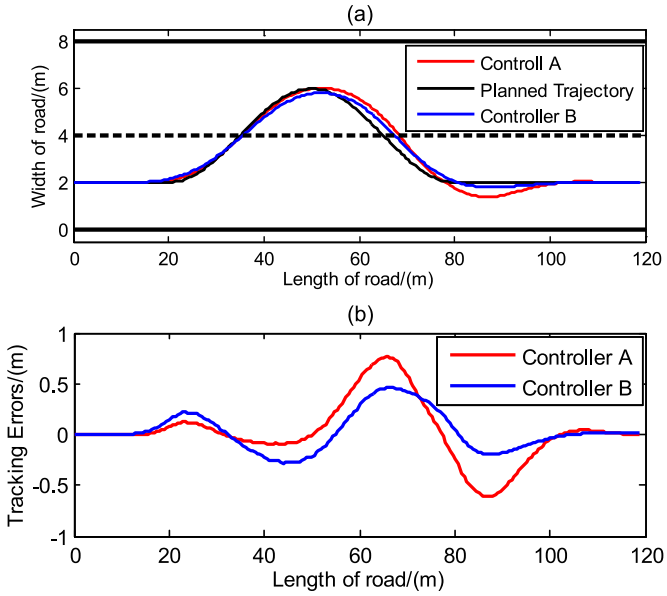

Fig. 14. Simulation results of path tracking. (a) Trajectory tracking. (b) Tracking errors.

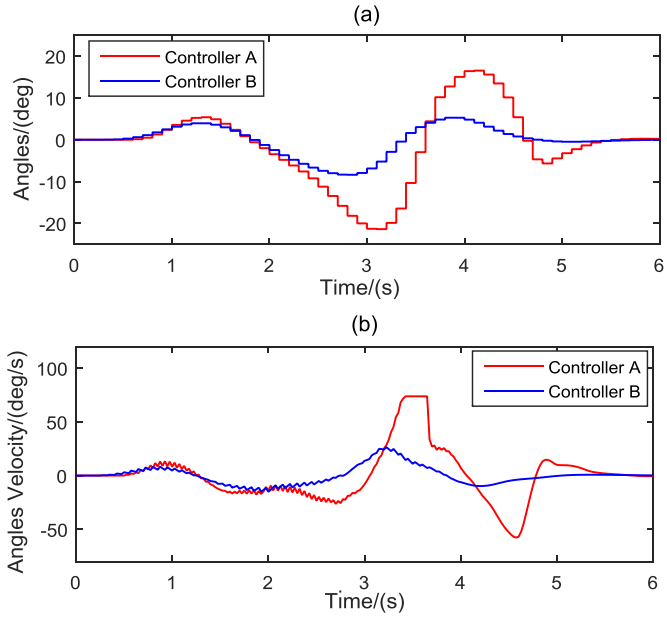

Fig. 15. Control inputs for MMPC. (a) Angles of front wheels. (b) Angle velocity of front wheels.

controller A. Controller B, with more constraints than controller A, employs smaller steering input commands and also generates smaller steering angle velocity, while controlling the vehicle, as shown in Fig. 15.

The better performance of controller B is also demonstrated by lower levels of yaw rate $(\dot{\psi})$ and sideslip angle of vehicle (β) than those of controller A. In the postmaneuver portion of the test $(t > 2.5\,\mathrm{s})$, controller A is able to steer the vehicle back into the linear region at the maximum steering rate and stabilizes the vehicle, as shown in Fig. 16. Controller B, because of the constraints on the steering angle, steering rate, yaw rate, and sideslip angle, always constrains the vehicle within the linear region.

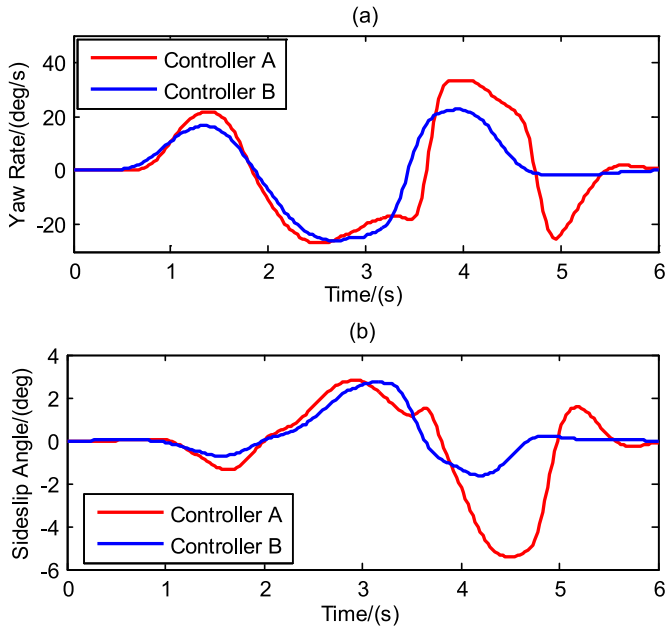

Fig. 16. Stability performance of collision avoidance system. (a) Yaw rates of vehicle. (b) Sideslip angles of vehicle.

The simulation results show that both controllers can make the vehicle track the planned trajectory. However, it should be pointed out that a good path-tracking performance with smooth front steering angle, yaw rate, and sideslip angle is obtained using controller B.

Scenario 2: To evaluate the performance of the path-planning program and the MMPC path-tracking controller, a moving obstacle with variable velocity, as shown in Fig. 13, is considered.

We set $\mu = 0.5$ for the friction coefficient in this scenario. Figs. 17–19 show the comparison between simulations for the two approaches at 20 m/s. Both controllers try to avoid the obstacle by steering to the left, forcing the vehicle to track the planned trajectory. Controller A becomes unstable, while controller B avoids the obstacle and is still able to track the planned trajectory.

Fig. 17 shows the trajectories and tracking errors of the vehicle, where the blue and red lines represent the simulation results of controller A and controller B, respectively, and the black curve is the planned trajectory computed by the path-planning program.

Controller A is able to keep the vehicle on the planned trajectory at the beginning of collision avoidance. However, once the vehicle deviates too far from the reference, the controller can no longer pull the system back to the planned trajectory, and the system becomes uncontrollable. This type of behavior is induced by tire saturation, which results in the sideslip angle and yaw rate of vehicle exceeding the bounds of the stability thresholds [36], as shown in Fig. 19.

We can improve the performance of controller A by extending the prediction horizon $N_p = 20$ and control horizon $N_c = 5$. However, this is done at the expense of computation time, and this generates runtime error on the described experimental platform.

In the postmaneuver portion of the test $(t > 4\,\mathrm{s})$, controller A could neither steer the vehicle to track the planned trajectory

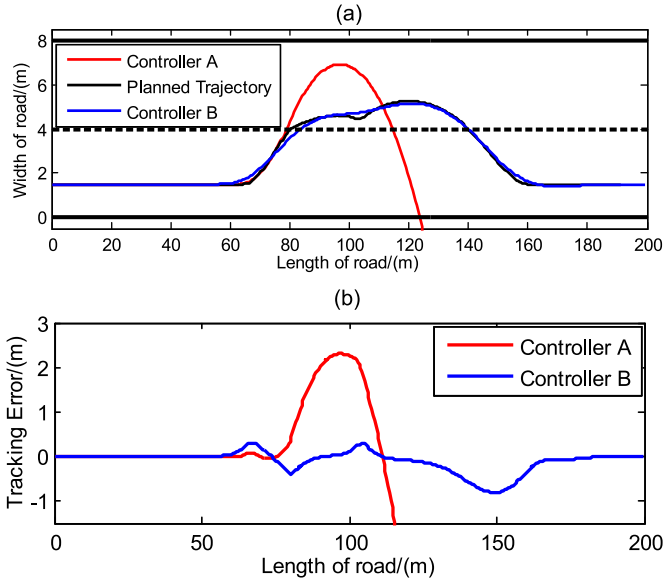

Fig. 17. Tracking performance of MMPC. (a) Planned trajectory and tracking trajectories. (b) Tracking errors.

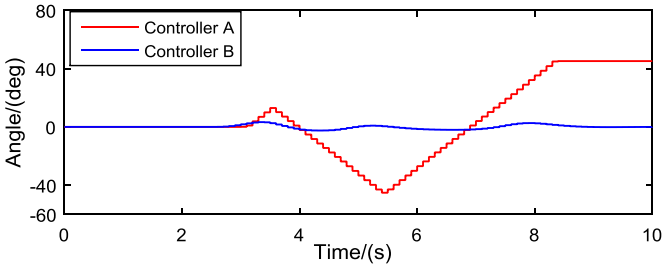

Fig. 18. Angles of front wheels for collision avoidance.

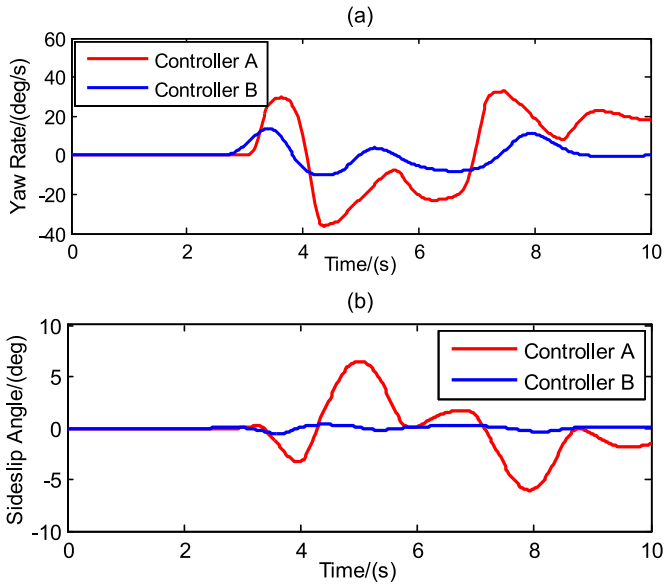

Fig. 19. Stability performance of vehicle. (a) Yaw rate of vehicle. (b) Sideslip angle of vehicle.

nor maintain stability even at the maximum steering angle and rate, as shown in Fig. 18. Controller B always constrains the vehicle within the linear region and leads to better tracking performance than controller A.

VII. Conclusion

In this paper, we have presented a framework for path planning and path tracking for a collision avoidance system of autonomous vehicles. The path-planning framework built a 3-D dangerous potential field based on the information of road and obstacles. A real-time collision-free trajectory was then generated for path tracking. As for the path-tracking framework, an optimal problem was formulated in terms of cost minimization under constraints in the MMPC method. The state constraints on lateral position, yaw rate, and sideslip angle and the input constraint on the steering wheel angle were proposed to stabilize the vehicle at high speeds. It is solved with Hildreth's quadratic programming procedure, and the constraints were incorporated in an augmented vehicle model.

The proposed path-tracking framework was implemented and tested in simulations. The MMPC approach was developed in MATLAB/Simulink, and the actual plant used in the simulations was a CarSim vehicle model. Simulation results demonstrate satisfactory tracking performance, in terms of collision avoidance, in both static and dynamic environments. The proposed controller was able to stabilize the vehicle on a low-friction-coefficient road and in the presence of a moving obstacle.

The promising results from the simulations motivated an effort to implement the proposed active safety system. Integration of collision avoidance control with environment information devices, such as radar and vision systems, is a topic of future research.

References

[1] S. Chang and T. J. Gordon, "A flexible hierarchical model-based control methodology for vehicle active safety systems," *Veh. Syst. Dyn.*, vol. 46, pp. 63–75, Sep. 2008.

[2] K. J. Yang, S. K. Gan, and S. Sukkarieh, "An efficient path planning and control algorithm for RUAV's in unknown and cluttered environments," *J. Intell. Robot. Syst.*, vol. 57, no. 1–4, pp. 101–122, Jan. 2010.

[3] M. P. Aghababa, "3D path planning for underwater vehicles using five evolutionary optimization algorithms avoiding static and energetic obstacles," *Appl. Ocean Res.*, vol. 38, pp. 48–62, Oct. 2012.

[4] J. Courbon, Y. Mezouar, N. Guenard, and P. Martinet, "Vision-based navigation of unmanned aerial vehicles," *Control Eng. Pract.*, vol. 18, no. 7, pp. 789–799, Jul. 2010.

[5] S. Saravanakumar and T. Asokan, "Multipoint potential field method for path planning of autonomous underwater vehicles in 3D space," *Intell. Serv. Robot.*, vol. 6, no. 4, pp. 211–224, Oct. 2013.

[6] V. Kunchev, L. Jain, V. Ivancevic, and A. Finn, *Path Planning and Obstacle Avoidance For Autonomous Mobile Robots: A Review*, ser. Lecture Notes in Computer Science, vol. 4252. Berlin, Germany: Springer-Verlag, 2006, pp. 537–544.

[7] Y. Kanayama and B. I. Hartman, "Smooth local path planning for autonomous vehicles," in *Proc. IEEE Int. Conf. Robot. Autom.*, 1989, vol. 1–3, pp. 1265–1270.

[8] Z. Shiller and Y. R. Gwo, "Dynamic motion planning of autonomous vehicles," *IEEE Trans. Robot. Autom.*, vol. 7, no. 2, pp. 241–249, Apr. 1991.

[9] A. K. Pamosoaji and K. S. Hong, "A path-planning algorithm using vector potential functions in triangular regions," *IEEE Trans. Syst., Man, Cybern., Syst.*, vol. 43, no. 4, pp. 832–842, Jul. 2013.

[10] A. Shum, K. Morris, and A. Khajepour, "Direction-dependent optimal path planning for autonomous vehicles," *Robot. Auton. Syst.*, vol. 70, pp. 202–214, Aug. 2015.

[11] P. Shi and Y. W. Zhao, "An efficient path planning algorithm for mobile robot using improved potential field," in *Proc. IEEE Int. Conf. ROBIO*, 2009, vol. 1–4, pp. 1704–1708.

[12] T. Shim, G. Adireddy, and H. L. Yuan, "Autonomous vehicle collision avoidance system using path planning and model-predictive-control-based

active front steering and wheel torque control," *Proc. Inst. Mech. Eng. D, J. Automobile Eng.*, vol. 226, no. D6, pp. 767–778, Jan. 2012.
[13] F. Rovira-Más and Q. Zhang, "Fuzzy logic control of an electrohydraulic valve for auto-steering off-road vehicles," *Proc. Inst. Mech. Eng. D, J. Automobile Eng.*, vol. 222, no. 6, pp. 917–934, Jun. 2008.
[14] S. H. Tabatabaei Oreh, R. Kazemi, and S. Azadi, "A sliding-mode controller for directional control of articulated heavy vehicles," *Proc. Inst. Mech. Eng. D, J. Automobile Eng.*, vol. 228, no. 3, pp. 245–262, Feb. 2014.
[15] K. Nam, S. Oh, H. Fujimoto, and Y. Hori, "Robust yaw stability control for electric vehicles based on active front steering control through a steer-by-wire system," *Int. J. Automotive Technol.*, vol. 13, no. 7, pp. 1169–1176, Dec. 2012.
[16] G. V. Raffo, G. K. Gomes, J. E. Normey-Rico, C. R. Kelber, and L. B. Becker, "A predictive controller for autonomous vehicle path tracking," *IEEE Trans. Intell. Transp.*, vol. 10, no. 1, pp. 92–102, Mar. 2009.
[17] W. Kim, D. Kim, K. Yi, and H. J. Kim, "Development of a path-tracking control system based on model predictive control using infrastructure sensors," *Veh. Syst. Dyn.*, vol. 50, no. 6, pp. 1001–1023, Jul. 2012.
[18] M. Hassanzadeh, M. Lidberg, M. Keshavarz, and L. Bjelkeflo, "Path and speed control of a heavy vehicle for collision avoidance manoeuvres," in *Proc. IEEE IV*, 2012, pp. 129–134.
[19] E. Kim, J. Kim, and M. Sunwoo, "Model predictive control strategy for smooth path tracking of autonomous vehicles with steering actuator dynamics," *Int. J. Automotive Technol.*, vol. 15, no. 7, pp. 1155–1164, Dec. 2014.
[20] L. Guo, P. S. Ge, M. Yue, and Y. B. Zhao, "Lane changing trajectory planning and tracking controller design for intelligent vehicle running on curved road," *Math. Probl. Eng.*, vol. 2014, pp. 1–9, Jan. 2014.
[21] D. B. Ren, J. Y. Zhang, J. Zhang, and S. Cui, "Trajectory planning and yaw rate tracking control for lane changing of intelligent vehicle on curved road," *Sci. China Technol. Sci.*, vol. 54, no. 3, pp. 630–642, Mar. 2011.
[22] X. L. Song, H. T. Cao, and J. Huang, "Vehicle path planning in various driving situations based on the elastic band theory for highway collision avoidance," *Proc. Inst. Mech. Eng. D, J. Automobile Eng.*, vol. 227, no. 12, pp. 1706–1722, Dec. 2013.
[23] M. T. Wolf and J. W. Burdick, "Artificial potential functions for highway driving with collision avoidance," in *Proc. IEEE Int. Conf. Robot. Autom.*, 2008, vol. 1–9, pp. 3731–3736.
[24] H. M. Choset, *Principles of Robot Motion: Theory, Algorithms, and Implementation*. Cambridge, MA, USA: MIT Press, 2005.
[25] R. Hayashi, J. Isogai, P. Raksincharoensak, and M. Nagai, "Autonomous collision avoidance system by combined control of steering and braking using geometrically optimised vehicular trajectory," *Veh. Syst. Dyn.*, vol. 50, pp. 151–168, Jan. 2012.
[26] G. P. Bevan, H. Gollee, and J. O'Reilly, "Trajectory generation for road vehicle obstacle avoidance using convex optimization," *Proc. Inst. Mech. Eng. D, J. Automobile Eng.*, vol. 224, no. D4, pp. 455–473, 2010.
[27] C. Pozna, F. Troester, R. E. Precup, J. K. Tar, and S. Preitl, "On the design of an obstacle avoiding trajectory: Method and simulation," *Math. Comput. Simul.*, vol. 79, no. 7, pp. 2211–2226, Mar. 2009.
[28] R. Rajamani,*Vehicle Dynamics and Control*. New York, NY, USA: Springer-Verlag, 2012.
[29] L. Wang, *Model Predictive Control System Design and Implementation Using MATLAB*. New York, NY, USA: Springer-Verlag, 2009.
[30] D. J. Cole, A. J. Pick, and A. M. C. Odhams, "Predictive and linear quadratic methods for potential application to modelling driver steering control," *Veh. Syst. Dyn.*, vol. 44, no. 3, pp. 259–284, Mar. 2006.
[31] X. X. Na and D. J. Cole, "Linear quadratic game and non-cooperative predictive methods for potential application to modelling driver-AFS interactive steering control," *Veh. Syst. Dyn.*, vol. 51, no. 2, pp. 165–198, Feb. 1, 2013.
[32] L. Del Re, F. Allgöwer, L. Glielmo, C. Guardiola, and I. Kolmanovsky, *Automotive Model Predictive Control Models, Methods and Applications*. New York, NY, USA: Springer-Verlag, 2010.
[33] U. Kiencke and L. Nielsen, *Automotive Control Systems for Engine, Driveline, and Vehicle*. New York, NY, USA: Springer-Verlag, 2005.
[34] D. A. Wismer and R. Chattergy, *Introduction to Nonlinear Optimization: A Problem Solving Approach*. New York, NY, USA: North Holland, 1979.
[35] A. N. Iusem and A. R. Depierro, "On the convergence properties of Hildreth quadratic-programming algorithm," *Math. Program.*, vol. 47, no. 1, pp. 37–51, May 1990.
[36] Y. Q. Gao, T. Lin, F. Borrelli, E. Tseng, and D. Hrovat, "Predictive control of autonomous ground vehicles with obstacle avoidance on slippery roads," in *Proc. ASME Dyn. Syst. Control Conf.*, 2010, vol. 1, pp. 265–272.

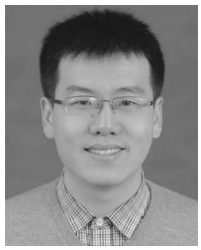

Jie Ji received the B.Sc. degree in mechanical engineering from the Chongqing Jiaotong University, Chongqing, China, in 2004 and the Ph.D. degree in mechanical engineering from Chongqing University in 2010.

Since July 2010, he has been an Associate Professor with the College of Engineering and Technology, Southwest University, Chongqing. From January 2014 to January 2015, he was a Postdoctoral Fellow with the Department of Mechanical and Mechatronics Engineering, University of Waterloo, Waterloo, ON, Canada. His current research interests include vehicle active safety systems, design/analysis of vehicle chassis control systems, and intelligent vehicles.

Dr. Ji has been a reviewer for several conferences related to path planning and tracking for intelligent vehicles.

Amir Khajepour received the Ph.D. degree from the University of Waterloo, Waterloo, ON, Canada, in 1996.

He is currently a Professor of mechanical and mechatronics engineering and the Canada Research Chair in "Mechatronic Vehicle Systems" with the University of Waterloo, where he also serves as the Waterloo Center for Automotive Research Executive Director. He is an expert in systems modeling and control of dynamic systems, and he has developed an extensive research program that applies his expertise to several key multidisciplinary areas. His research has resulted in several patents, technology transfers, and two startup companies. He has authored or coauthored more than 350 journal and conference publications, as well as five books and seven book chapters.

Dr. Khajepour is a Fellow of the Engineering Institute of Canada and the American and Canadian Society of Mechanical Engineering. He received the Engineering Medal from Professional Engineers Ontario. He is an Associate Editor of the *International Journal of Vehicle Autonomous Systems* and the *International Journal of Powertrains*.

Wael William Melek (M'02–SM'06) received the M.A.Sc. and Ph.D. degrees in mechanical engineering from the University of Toronto, Toronto, ON, Canada, in 1998 and 2002, respectively.

Between 2002 and 2004, he was the Artificial Intelligence Division Manager with Alpha Global IT, Inc., Toronto. He is currently an Assistant Professor with the Department of Mechanical Engineering, University of Waterloo, Waterloo, ON. His current research interests include mechatronics applications, robotics, industrial automation and the application of fuzzy logic, neural networks, and genetic algorithms for modeling and control of dynamic systems.

Dr. Melek is a member of the American Society of Mechanical Engineers.

Yanjun Huang received the M.S. degree in vehicle engineering from Jilin University, Changchun, China, in 2012. He is currently working toward the Ph.D. degree with the University of Waterloo, Waterloo, ON, Canada.

He is working on advanced control strategies and their real-time applications; heating, ventilating, and air conditioning (HVAC) nonlinear dynamic system modeling and control; and modeling of hybrid powertrains, components sizing, and power management control strategy design through concurrent optimization and hardware-in-the-loop testing.